Modification of meso-micromixing interaction reaction model in the continuous reactors

Junan Jiang, Ning Yang, Hanyang Liu, Jianxin Tang, Chenfeng Wang, Rijie Wang, Xiaoxia Yang

Contents

Accuracy Verification and Mesh Independent Test

The principle of Villermaux−Dushman Method

The principle of Gaussian process regression and Bayesian optimization

The raw data for multi-objective optimization

Nomenclature

References

1. Accuracy Verification and Mesh Independence Test

1.1 Accuracy Verification

1.1.1 Turbulence Model

To verify the reliability of the simulation, the pressure drop in the fully developed section of a reactor with specific parameters was obtained by both experiments and simulations. The results indicate that the maximum deviation for pressure drop is 4.5%. Therefore, the reliability of the used algorithm was verified. The non-ideal flow causes the fluid to consume a small amount of additional energy as it passes through the bends and joints in the experiment, so the experimental values are always a little larger than those of the simulations.
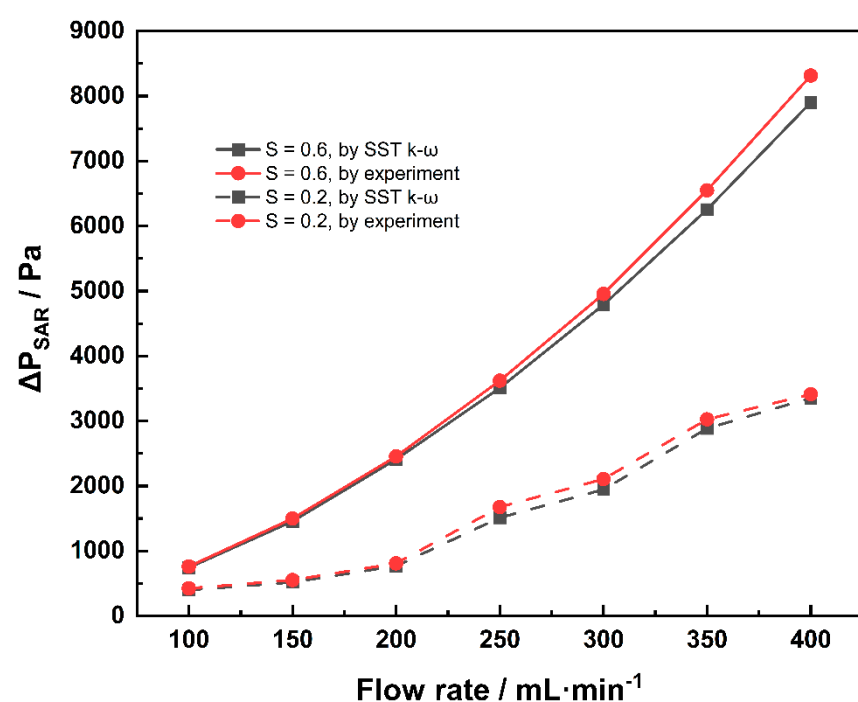
Figure S1 Verification of the numerical and experimental results about the pressure drop of both S = 0.2 and S = 0.6, with different flow rates.

1.1.2 Validation between micromixing time results in CFD simulation and experiments

To further verify the accuracy of selected model, we also test the micromixing time under different conditions by both experiments and simulations. It aims to check if it is responsible to use numerical simulation to acquire the micromixing time, since many, 100 sets of results for multi-objective optimization should be acquired. However, this can be also used to check if the model is appropriate. The error limits for both were set at ±25% according to J.M. Commenge's study[1]. According to the results, the maximum relative deviation is 13.48% while the minimum one is 0.24%. Therefore, SST k-ω turbulent model can meet the demand to calculate.
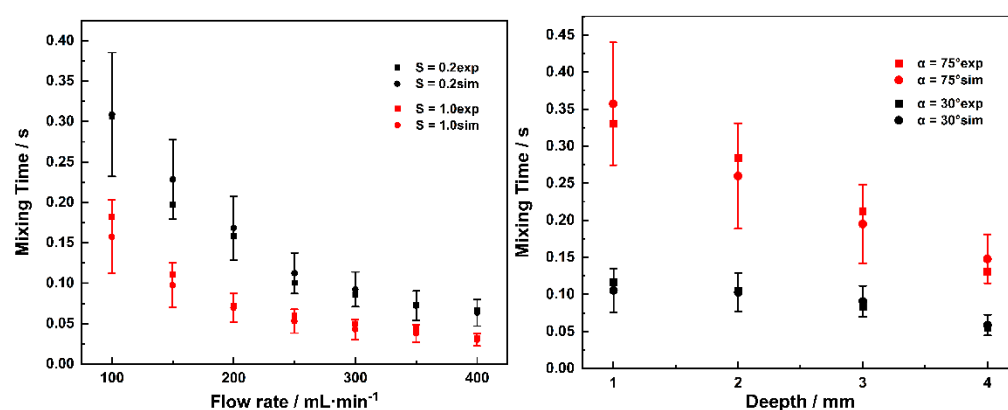
Figure S2 Error lines of mixing time with different parameters: (a) cases with changing flow rates and skewness; (b) cases with changing groove depth and circulation angles. Here, the square and circle symbols represent experimental and simulation results, respectively.

1.2 Mesh Independence Test

Concentration and energy dissipation rate are more difficult parameters to calculate accurately for simulations of split-and-recombine millimeter-scale reactors, since more and higher quality discrete grids are required to simulate these parameters. Therefore, steady-state simulations of SAR reactors with a specific structure and appropriate flow rates were used to complete the grid independence test, $\alpha=45°$, d=3 mm, S=0.4, L_G=10 mm, and F=300 mL/min. The criteria evaluated were the overall reactor pressure drop, viscous dissipation rate (VDR), and UIAW along the reactor axial direction at 35 mm. The results are shown in Table S1.
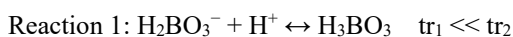
Table S1 Grid independence test

Grid No.	Grid Number	ΔP, Pa	Relative Error-ΔP	VDR, W/kg	Relative Error-VDR	UIAW	Relative Error-UIAW
1	5255206	49.2548	-	$1.5965*10^{-5}$	-	0.8497	-
2	6151520	49.3533	0.199%	$1.6039*10^{-5}$	0.464%	0.8339	1.86%
3	7340895	49.3340	0.0391%	$1.6072*10^{-5}$	0.206%	0.8422	0.995%
4	8849516	49.3365	0.00507%	$1.6101*10^{-5}$	0.180%	0.8450	0.332%

All the relative error was calculated from the results of the grid in a certain row corresponding to the ones of the previous row. Therefore, when the relative error from one grid number is quite low, we can choose that to simulate. From Table S1, the relative errors of pressure drop and VDR between grid 3 and 4 are similar. In one hand, the relative errors in grid 3 are all less than 1%, which can meet the requirement of calculation accuracy. In the other hand, it will cost much more time to simulate one case using grid 4. Hence, grid 3 with grid number 7340895 was chosen to conduct the simulations.

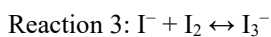A hybrid mesh with a tetrahedral mesh as the primary was generated. The overall grid size of the annular gap and mixing structure was 0.16mm. And the grid was refined at the wall surface, with the growth rate of boundary layers 1.1 and the numbers of boundary layers of 5. All the grids obtained have the skewness less than 85%, which meets the needs of grid quality.

2. The principle of Villermaux−Dushman Method[2-4]

In this method, borate neutralization is quasi-instantaneous with characteristic time tr1; the second, the Dushman reaction is slower and has characteristic time tr2 close to the mixing time tm. The balanced reactions can be modeled as follows:

Reaction 1: $H_2BO_3^- + H^+ \leftrightarrow H_3BO_3$ $tr_1 \ll tr_2$

Reaction 2: $5I^- + IO_3^- + 6H^+ \leftrightarrow 3I_2 + 3H_2O$ $tr_2 \approx t_m$

The iodine I2 further reacts with iodide ions I^-, yielding I_3^- ions following the quasi-instantaneous equilibrium reaction:

Reaction 3: $I^- + I_2 \leftrightarrow I_3^-$

The principle of this method is to add, in stoichiometric deficit, a small amount of H^+ to the initial I^-, IO_3^- and $H_2BO_3^-$. When sufficient micromixing is achieved in the reactor, the added H^+ will be completely consumed by reaction 1, so that no I_2 and subsequent I_3^- produced. On the other hand, when the mixing process is not sufficiently fast to sustain reaction 1, the local overconcentration of H^+ produces I_2 by reaction 2, which reacts with I^- to yield I_3^-. Therefore, it is necessary to use a UV-vis spectrometer at a wavelength of 353 nm to determine the concentration of I_3^- generated in the system and obtain the concentration of various ions. The following equation is used to calculate the Segregation Index (X_S), an important parameter for evaluating the micromixing performance. X_S ranges between 0 (complete micromixing) and 1 (no micromixing), so it can be used to characterize the degree of micromixing.

$$X_S = \frac{Y}{Y_{ST}} = \frac{2([I_2] + [I_3^-])}{[H^+]_0}\left(\frac{Q_p}{Q_{H^+}} + 1\right)\left(\frac{[H_2BO_3^-]}{6[IO_3^-]_0} + 1\right) \tag{1}$$

where Q_i denotes the molar flow rate of component i, [j] the concentration of component j, and the subscript 0 denotes the original reaction mixture. According to the conventional definition, Y is the ratio of the quantity of H^+ transformed into I_2 following the second reaction to the total quantity of injected H^+ and Y_{ST} is the value of Y in the case of total segregation.

The mass balance on I2 leads to the following expression:

$$[I_2]^2 - \left(\left(\frac{3}{5}\right)[I^-]_0 - \frac{8}{5}[I_3^-]\right)[I_2] + \frac{3}{5}\frac{[I_3^-]}{5K_B} = 0 \tag{2}$$

where K_B is the equilibrium constant of reaction 3 which depends on the solution temperature:

$$log_{10} K_B = \frac{555}{T} + 7355 - 2575 \, log_{10}(T) \tag{3}$$

For conducting the experiments, two solutions were prepared. The sulfuric acid solution was equipped separately. Another buffer solution containing boric acid and sodium hydroxide was added to the mixed solution of potassium iodide and potassium iodate to form a single homogeneous solution. The purpose of adding the buffer solution was to prevent iodate and iodide react with H^+ of boric acid in the solution.

In order to obtain the mixing time, an incorporation model in terms of micromixing is introduced. The basic theory of this model is [5]: two fluids enter the reactor at the same time and one of them is dispersed into numerous tiny fluid clusters, which in turn incorporate and react with the other fluid. When the incorporation rate is constant, the controlling equation of this model is

$$\frac{dC_j}{dt} = \left(C_{j_0} - C_j\right)\frac{1}{g}\frac{dg}{dt} + R_j \tag{4}$$

where C_{j0} is the initial concentration of component j, C_j the concentration at time t and R_j the incorporation rate of component j. g(t) depends on the incorporation model mechanism and represents the volume growth of the fluid, which is expressed as

$$g(t) = exp\left(\frac{t}{t_m}\right) \tag{5}$$

Combining these three reactions, the kinetic equations for each ion can be obtained. A series of t_m is substituted into ODEs (Eqn. (4)) solved by fourth-order Runge-Kutta method. When H^+ concentration is less than 0, the iteration stops. The following algorithm was implemented using a self-programmed MATLAB: assuming a t_m first, the corresponding $X_S^`$ can be obtained. When the

difference between the experimental value (X_S) and calculated one ($X_S^{'}$) satisfies the error limit, the iteration stops, obtaining t_m, otherwise goes into the next round of calculation until the error limit is satisfied.

3. The principle of Gaussian process regression and Bayesian optimization

Gaussian process regression (GPR) is a widely accepted surrogate model. The core criterion of Gaussian process regression is that any finite combination of linear functions obeys a joint Gaussian distribution. This process cannot obtain a specific function form. Conversely, it enables all the sample points to pass through the fitting function and narrow the value range of each dependent variable so that it is closer to the Gaussian distribution with the maximum probability density. Finally, a set of predicted values can be obtained with the highest R^2 and lowest MSE.

Assume that there are many sample points ($\mathbf{x}^*$, $\mathbf{y}^*$). Note that $\mathbf{x}^*$ and $\mathbf{y}^*$ should be vectors. These are used to predict the new generation of independent and dependent variables, named $\mathbf{x}$ and $\mathbf{f}$. ($\mathbf{x}^*$, $\mathbf{y}^*$) and ($\mathbf{x}$, $\mathbf{f}$) should jointly obey the multivariate Gaussian distribution, shown in Eq. (6), where μ_f, μ_y are the mean functions of the predicted and observed values, respectively. $\begin{bmatrix} K_{ff} & K_{fy} \\ K_{fy}^T & K_{yy} \end{bmatrix}$ is the kernel function, which is RBF function (Eq. (7)) in this study.

Then, Eq. (8) can act as a posterior distribution to get the $\mathbf{f}$ and the shape of regression curve. This curve is called surrogate function. It allows us to acquire a certain distribution about the function, and any function acquired by sampling on that distribution can be a mapping between the dependent and independent variables.

$$\begin{bmatrix} \boldsymbol{f} \\ \boldsymbol{y}^* \end{bmatrix} \sim \mathcal{N}\left(\begin{bmatrix} \boldsymbol{\mu}_f \\ \boldsymbol{\mu}_y \end{bmatrix}, \begin{bmatrix} K_{ff} & K_{fy} \\ K_{fy}^T & K_{yy} \end{bmatrix} \right) \tag{6}$$

$$\begin{bmatrix} K_{ff} & K_{fy} \\ K_{fy}^T & K_{yy} \end{bmatrix} = \sigma^2 \, exp\left(-\frac{\| \, x_i - x_j \, \|_2^2}{2l^2} \right) \tag{7}$$

$$\boldsymbol{f}|\boldsymbol{x}^*, \boldsymbol{y}^* \sim \mathcal{N}(K_{fy}^T K_{ff}^{-1} \boldsymbol{y} + \boldsymbol{\mu}_f, K_{yy} - K_{fy}^T K_{ff}^{-1} K_{fy}) \tag{8}$$

In addition to regression, the Gaussian process can be also applied to optimize, i.e. Bayesian optimization. After obtaining the surrogate model, we can use an acquisition function to find the expected $\mathbf{x}$ when the function values are minimum. Assuming that in the sample, the minimum $\mathbf{y}'$ occurs at the point $\mathbf{x}'$. To find the new generation of minimum $\mathbf{y}$ is equivalent to maximizing $\mathbf{y}'$-$\mathbf{y}$, so the difference can be expressed as

$$I(\boldsymbol{x}) = max(\boldsymbol{y}' - \boldsymbol{y}, \boldsymbol{0}) \tag{9}$$

As a result, finding the minimum of y means maximum $I(\boldsymbol{x})$, therefore, the expectation of $I(\boldsymbol{x})$ is a typical acquisition function, which can be represented as:

$$EI(\boldsymbol{x}) = (\boldsymbol{y}' - \boldsymbol{\mu})\Phi\left(\frac{\boldsymbol{y}' - \boldsymbol{\mu}}{\sigma} \right) + \sigma\phi\left(\frac{\boldsymbol{y}' - \boldsymbol{\mu}}{\sigma} \right) \tag{10}$$

For each $\mathbf{x}$, we get two hyperparameters $\boldsymbol{\mu}$ and σ through Gaussian process. These two hyperparameters are substituted to Eq. (8) to find $\mathbf{x}$ corresponding to the maximum value of EI.

4. The raw data for multi-objective optimization

The data including 100 sets of design points, mesomixing and micromixing characteristic time, pressure drop and two yields is presented in Table S3.

Table S3 The raw data for multi-objective optimization

	T	α	d	F	t_d	t_m	ΔP_{SAR}	Y_1	Y_2
DP1	0.424	72.9	2.88	399.22	0.01715	0.09113	1726.65	0.374	0.557
DP2	0.719	25.9	3.14	287.18	0.00704	0.03109	20488.75	0.238	0.704
DP3	0.295	57.2	4.57	315.90	0.00707	0.04456	6216.24	0.593	0.305
DP4	0.785	52.5	4.91	119.35	0.00730	0.05597	8203.02	0.547	0.375
DP5	0.674	31.0	2.00	203.72	0.01598	0.07907	4359.80	0.140	0.828
DP6	0.580	21.1	1.35	216.02	0.01370	0.06008	7748.70	0.090	0.888
DP7	0.373	16.8	1.73	262.40	0.01064	0.04370	12217.60	0.112	0.861
DP8	0.730	62.5	1.50	139.32	0.04319	0.27511	480.13	0.267	0.699
DP9	0.873	68.5	4.26	150.86	0.01254	0.08907	3297.06	0.859	0.102
DP10	0.637	43.9	3.50	357.88	0.00804	0.03877	10096.89	0.357	0.563
DP11	0.280	35.5	2.71	374.51	0.01217	0.05716	4570.42	0.263	0.675
DP12	0.458	64.9	2.07	331.63	0.02297	0.12017	1222.83	0.266	0.684
DP13	0.975	49.2	2.53	185.59	0.01751	0.09706	3101.37	0.209	0.750
DP14	0.544	36.0	4.75	353.20	0.00326	0.01676	42053.72	0.585	0.299
DP15	0.933	47.2	2.35	302.87	0.01196	0.05641	6446.60	0.234	0.713
DP16	0.487	56.2	3.38	222.37	0.01812	0.11045	1723.03	0.331	0.613
DP17	0.214	18.6	1.11	277.16	0.01319	0.05456	7436.49	0.102	0.872
DP18	0.915	40.6	4.06	171.77	0.00850	0.05017	9985.26	0.302	0.632
DP19	0.839	70.8	3.81	247.27	0.01160	0.06949	4085.64	0.468	0.463
DP20	0.355	28.7	3.72	112.96	0.01879	0.12748	2008.99	0.448	0.501
DP21	0.444	63.5	1.22	228.49	0.03845	0.21911	501.93	0.199	0.769
DP22	0.364	60.4	1.18	328.86	0.02896	0.14832	818.34	0.208	0.751
DP23	0.682	16.1	2.47	158.65	0.01076	0.05023	13544.42	0.087	0.891

DP24	0.509	32.4	4.02	210.36	0.00857	0.04847	8631.39	0.301	0.631
DP25	0.208	58.2	2.97	164.64	0.03725	0.26341	367.48	0.859	0.122
DP26	0.870	25.3	4.83	266.93	0.00228	0.01112	125746.67	0.531	0.358
DP27	0.408	52.2	3.92	358.95	0.00876	0.04781	5807.23	0.455	0.452
DP28	0.676	21.0	4.41	260.94	0.00351	0.01678	60782.57	0.409	0.498
DP29	0.563	50.6	3.11	342.46	0.01181	0.05955	4562.41	0.316	0.615
DP30	0.826	38.7	4.37	130.50	0.00902	0.05935	8058.49	0.351	0.584
DP31	0.793	42.1	3.48	107.16	0.02020	0.13750	2011.32	0.865	0.101
DP32	0.521	66.6	4.64	383.30	0.00509	0.02961	12857.03	0.642	0.247
DP33	0.739	55.0	3.31	308.30	0.01099	0.05724	5387.90	0.332	0.597
DP34	0.632	46.4	1.43	294.81	0.01882	0.08955	2599.15	0.172	0.789
DP35	0.957	69.4	3.77	322.42	0.00831	0.04438	8532.65	0.412	0.501
DP36	0.971	18.8	2.66	239.77	0.00636	0.02640	37016.11	0.168	0.791
DP37	0.894	28.7	1.78	180.36	0.01476	0.07207	6150.48	0.125	0.846
DP38	0.340	40.6	2.34	389.08	0.01390	0.06468	3599.39	0.254	0.688
DP39	0.285	74.6	2.00	118.89	0.07359	0.55721	118.06	0.591	0.221
DP40	0.259	34.0	2.09	198.15	0.02604	0.14617	1157.14	0.159	0.808
DP41	0.267	37.2	3.79	393.78	0.00782	0.03941	7957.32	0.420	0.488
DP42	0.739	66.3	3.88	288.31	0.00995	0.05715	5237.69	0.439	0.478
DP43	0.762	58.2	2.75	242.37	0.01750	0.09636	2421.57	0.256	0.693
DP44	0.512	34.7	1.97	303.69	0.01419	0.06512	4626.00	0.176	0.782
DP45	0.387	22.7	2.36	224.76	0.01356	0.06463	5734.72	0.134	0.834
DP46	0.567	62.0	4.64	217.37	0.00763	0.05157	6418.51	0.563	0.348
DP47	0.436	41.1	4.44	142.39	0.01132	0.08025	3717.34	0.491	0.444

DP48	0.670	51.9	1.25	177.52	0.03252	0.18465	891.81	0.164	0.808
DP49	0.450	42.3	4.07	158.89	0.01379	0.09292	2754.81	0.439	0.501
DP50	0.332	71.9	2.51	333.46	0.02515	0.14215	812.91	0.333	0.614
DP51	0.828	25.8	3.49	172.98	0.00874	0.04531	13645.41	0.178	0.779
DP52	0.916	27.2	4.94	372.67	0.00151	0.00676	257749.04	0.659	0.221
DP53	0.534	17.7	3.39	263.81	0.00619	0.02712	27566.44	0.230	0.714
DP54	0.616	31.2	4.22	352.83	0.00425	0.02016	33505.91	0.468	0.430
DP55	0.870	50.6	1.44	315.52	0.01579	0.07319	3847.37	0.195	0.761
DP56	0.923	19.4	2.91	270.49	0.00562	0.02296	43130.96	0.209	0.739
DP57	0.217	57.0	3.05	191.66	0.03072	0.20656	531.30	0.498	0.456
DP58	0.686	64.6	1.17	100.42	0.06237	0.43308	251.02	0.052	0.937
DP59	0.983	73.2	2.06	361.98	0.01551	0.07493	3303.25	0.263	0.680
DP60	0.283	47.8	1.80	126.25	0.05177	0.35047	284.94	0.416	0.427
DP61	0.644	55.8	3.42	254.04	0.01364	0.07681	3338.08	0.320	0.616
DP62	0.435	16.3	1.50	145.09	0.01692	0.08071	5743.31	0.055	0.932
DP63	0.845	38.0	2.60	199.28	0.01431	0.07501	4792.41	0.198	0.760
DP64	0.222	21.6	2.78	326.83	0.00948	0.04181	9717.52	0.218	0.729
DP65	0.524	42.8	1.10	178.33	0.03137	0.17352	984.06	0.131	0.844
DP66	0.340	48.9	1.60	364.95	0.02056	0.09894	1675.47	0.219	0.734
DP67	0.838	57.1	4.57	161.44	0.00820	0.05631	7222.50	0.516	0.408
DP68	0.480	53.5	3.97	319.64	0.00901	0.05072	5616.41	0.451	0.460
DP69	0.252	70.5	2.33	296.24	0.03184	0.18919	494.05	0.346	0.608
DP70	0.731	47.9	1.36	287.62	0.01854	0.08885	2722.47	0.178	0.782
DP71	0.634	30.8	2.12	114.50	0.02657	0.15823	1648.65	0.183	0.788

DP72	0.931	34.7	4.93	221.82	0.00287	0.01607	65607.64	0.527	0.363
DP73	0.496	39.0	1.87	385.05	0.01296	0.05669	5074.24	0.219	0.730
DP74	0.767	64.0	3.39	373.67	0.00963	0.04892	6295.63	0.400	0.517
DP75	0.301	29.2	2.97	243.02	0.01378	0.07133	4003.21	0.293	0.653
DP76	0.965	74.6	4.38	343.50	0.00544	0.03038	15390.49	0.557	0.336
DP77	0.365	61.3	3.80	130.59	0.02716	0.21045	638.69	0.826	0.152
DP78	0.711	18.4	3.03	206.72	0.00779	0.03528	21096.15	0.155	0.807
DP79	0.897	66.5	4.71	278.68	0.00463	0.02787	19241.36	0.579	0.311
DP80	0.589	25.8	4.06	120.68	0.01094	0.06892	6590.19	0.266	0.683
DP81	0.463	18.3	2.18	323.62	0.00795	0.03155	19398.13	0.179	0.777
DP82	0.597	72.6	1.07	199.16	0.04312	0.25430	429.61	0.185	0.787
DP83	0.659	67.7	2.63	359.85	0.01581	0.08043	2579.95	0.307	0.630
DP84	0.753	23.9	2.55	145.16	0.01432	0.07462	6323.58	0.121	0.851
DP85	0.202	34.3	3.26	119.00	0.02951	0.20816	732.61	0.670	0.226
DP86	0.420	38.6	2.31	208.68	0.02195	0.12031	1684.04	0.181	0.782
DP87	0.797	15.3	4.72	180.85	0.00277	0.01370	118494.15	0.367	0.548
DP88	0.892	45.9	4.00	393.93	0.00473	0.02222	27725.07	0.477	0.421
DP89	0.840	30.0	1.57	344.57	0.00935	0.03775	13869.73	0.186	0.769
DP90	0.536	24.8	3.19	241.69	0.00920	0.04428	10894.30	0.206	0.744
DP91	0.386	50.7	4.50	333.04	0.00613	0.03598	9506.96	0.562	0.332
DP92	0.246	28.9	3.70	138.59	0.01776	0.11673	2001.42	0.247	0.707
DP93	0.945	55.6	1.67	378.09	0.01301	0.05773	5468.86	0.229	0.718
DP94	0.617	65.5	3.43	229.00	0.01710	0.10455	1917.05	0.376	0.566
DP95	0.981	43.8	4.94	277.20	0.00260	0.01420	70870.72	0.606	0.277

DP96	0.305	52.0	1.94	253.32	0.02889	0.16147	797.60	0.215	0.746
DP97	0.681	69.6	2.84	172.07	0.02850	0.18528	819.27	0.496	0.457
DP98	0.502	39.2	4.31	293.69	0.00601	0.03283	13642.21	0.449	0.455
DP99	0.360	57.8	1.36	306.32	0.02865	0.14912	849.18	0.199	0.761
DP100	0.805	62.5	4.16	108.26	0.01796	0.13903	1736.60	0.204	0.782

5. Nomenclature

ANN	Artificial neural network for short
BO	Bayesian optimization for short
c_i	The mole concentration of component i, mol/m³
d	Groove depth, mm
D	The hydrodynamic diameter of the reactor cross section, m
E	The engulfment rate in terms of micromixing, s⁻¹
EDR	Energy dissipation rate for short
F	Flow rate, mL/min
GPR	Gaussian process regression for short
L_G	Distance between two mixing elements, mm
L_M	Length of a mixing element, mm
MSE	Mean square error for short
P	Local pressure field, Pa
ΔP_{SAR}	Pressure drop in the full domain of reactors
r_i	Intrinsic reaction rate of component i, mol/(m³·s)
R_I	Outer radius of tube-in-tube reactors, mm
R_O	Inner radius of tube-in-tube reactors, mm
R^2	Coefficient of determination
Re	Reynold number
S	Skewness of curved grooves
SAR	Split-and-recombine reactor for short
t_d	Mesomixing characteristic time, s
t_m	Micromixing characteristic time, s
u	Local velocity field, m/s
u_m	Average velocity along the flow direction, m/s
V	Volume of the reactor fluid domain
X_0	Ratio of initial flow rates in a tubular reactor
X_B	Volume of micromixed fluid relative to the whole fluid
X_u	Volume fraction which contains the partially segregated fluid as islands, embedded in a sea
Y_1	Intermediate product yield

Y_2	Final product yield	
z	Axial position of the reactors, m	

Greek symbols		
α	Circulation angle, °	
ε	Energy dissipation rate, m^2/s^3	
Λ_c	Average from the integral scale of concentration fluctuations to Kolmogorov scale	
μ	Dynamic viscosity of the fluid, Pa·s	
ν	Kinematic viscosity of the fluid, Pa·s	
ρ	Density of the fluid, kg/m^3	
φ_B	Ratio of fluid volume change after micromixing	

6. References

1. Commenge, J.-M. and L. Falk, Villermaux–Dushman protocol for experimental characterization of micromixers. Chemical Engineering and Processing: Process Intensification, 2011. **50**(10): p. 979-990.

2. Ghanem, A., et al., Static mixers: Mechanisms, applications, and characterization methods - A review. Chemical Engineering Research & Design, 2014. **92**(2): p. 205-228.

3. Arian, E. and W. Pauer, A comprehensive investigation of the incorporation model for micromixing time calculation. Chemical Engineering Research and Design, 2021. **175**: p. 296-308.

4. Wenzel, D., et al., On the reactant concentration and the reaction kinetics in the Villermaux-Dushman protocol. Chemical Engineering and Processing - Process Intensification, 2018. **130**: p. 332-341.

5. Fournier, M.C., L. Falk, and J. Villermaux, A new parallel competing reaction system for assessing micromixing efficiency—Experimental approach. Chemical Engineering Science, 1996. **51**(22): p. 5053-5064.